

# Broadband measurements of ocean surface topography using airborne lidar technology

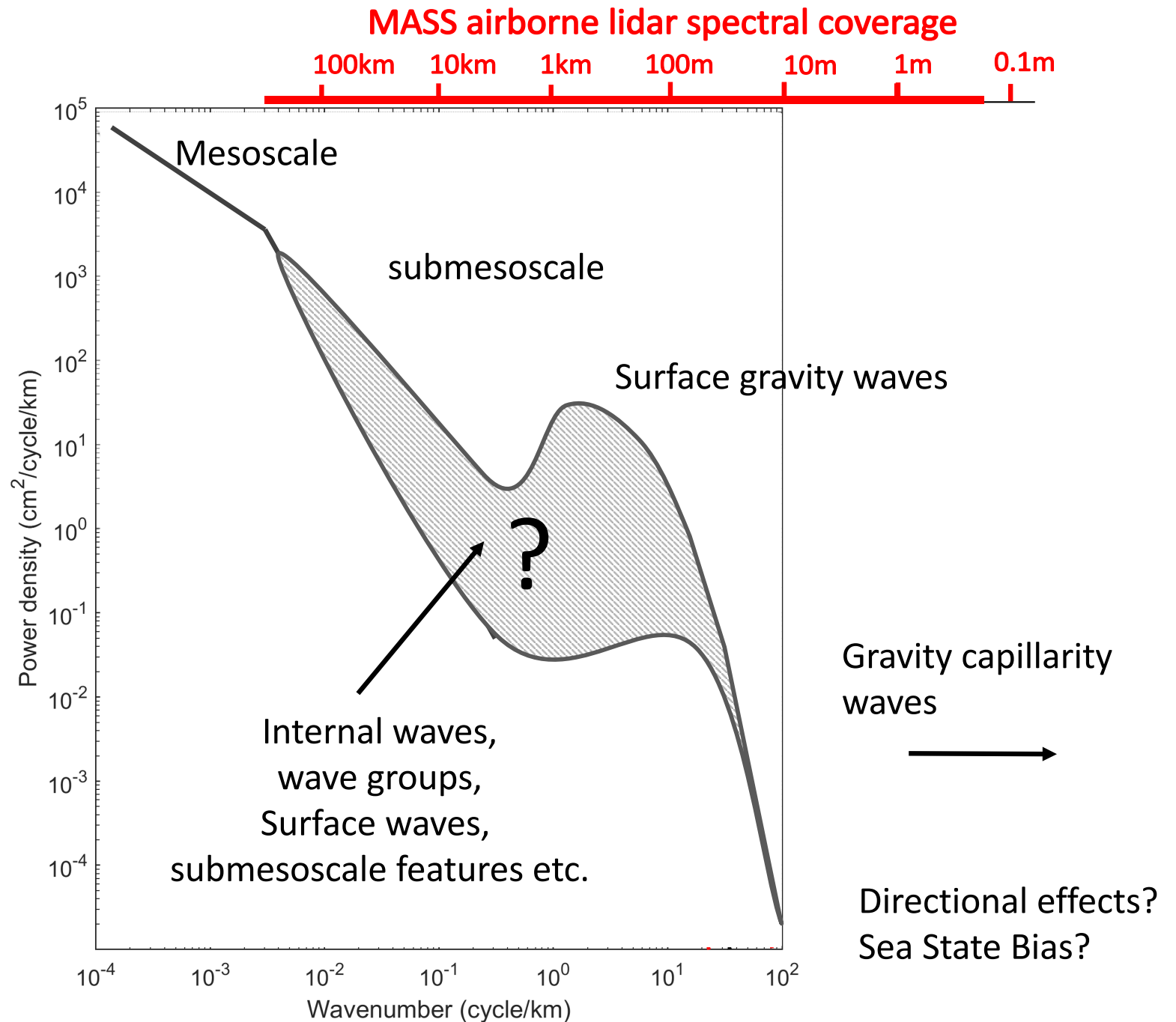
Luc Lenain & Ken Melville

Scripps Institution of Oceanography, UCSD

June 27 2018

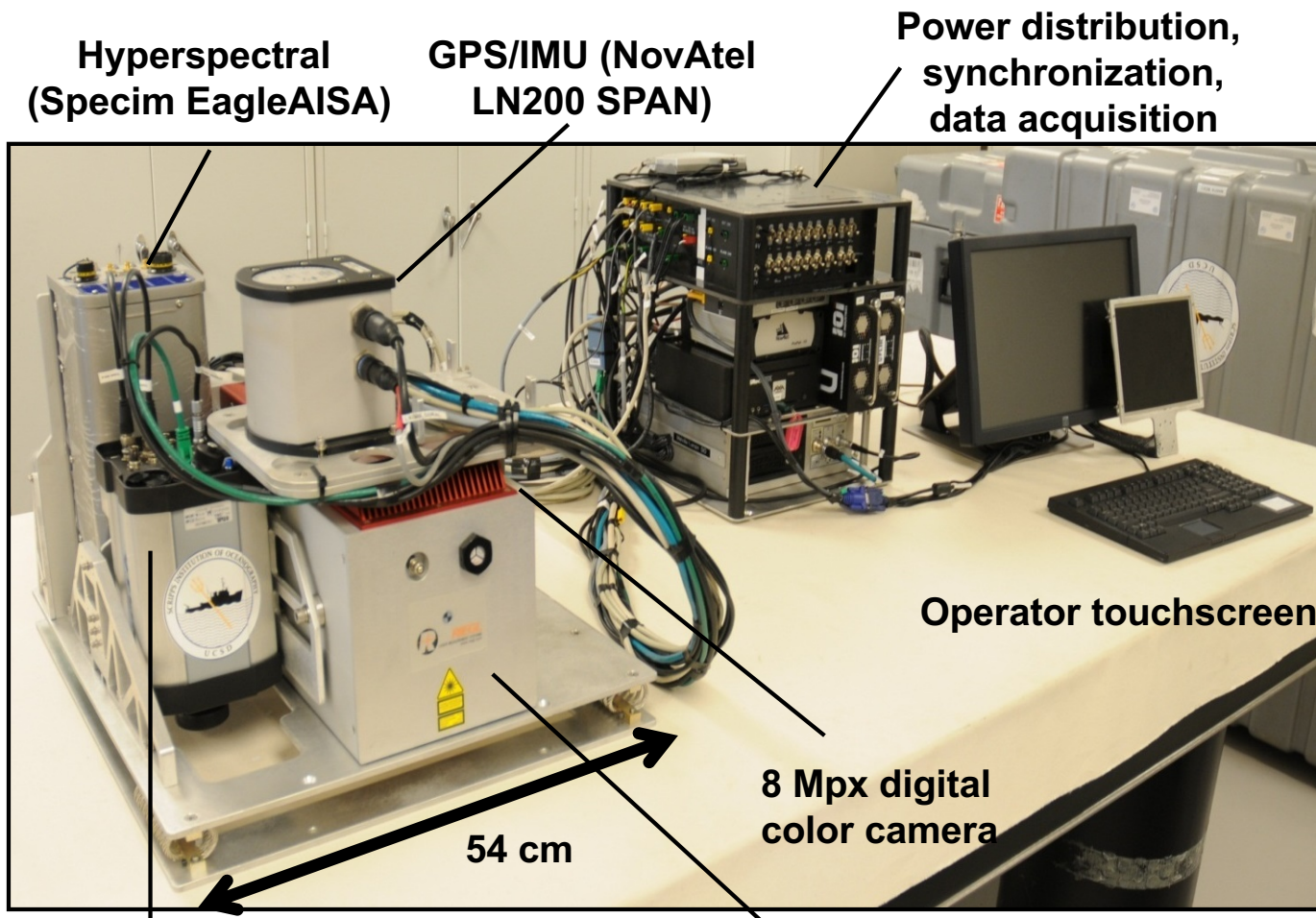
- **Airborne lidar measurements of sea surface topography ranging from submeter- to meso- scales**
- **Implications for future high resolution satellite altimeters and the role of airborne lidar technology for the SWOT CALVAL.**





MASS: Modular Aerial Sensing System (Melville et al. 2016, JTECH)

# SIO Modular Aerial Sensing System (MASS)

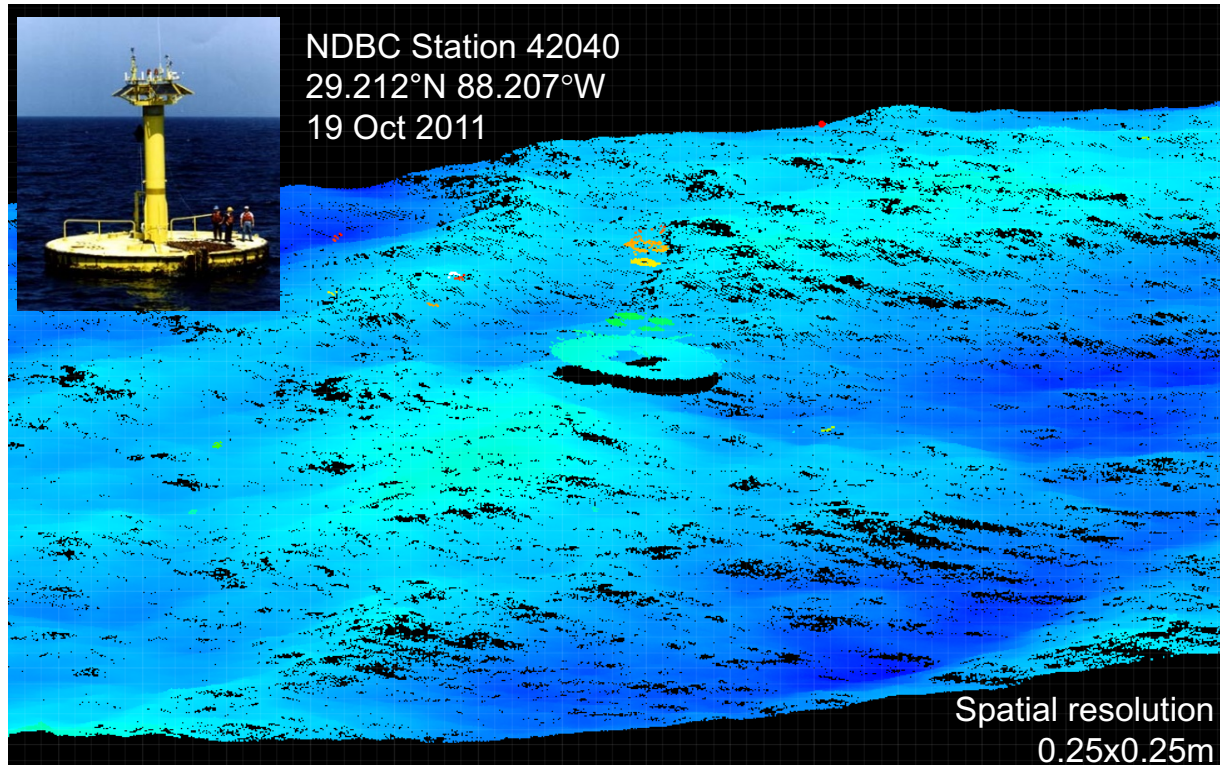


**Long Wave IR Camera (FLIR SC6000 LWIR)**

**Scanning waveform lidar (RIEGL Q680i)**



Melville, W.K., L. Lenain, D.R. Cayan, M. Kahru, J.P. Kleissl, P.F. Linden, and N.M. Statom, 2016: [The Modular Aerial Sensing System](https://doi.org/10.1175/JTECH-D-15-0067.1). *J. Atmos. Oceanic Technol.*, 33, 1169–1184, <https://doi.org/10.1175/JTECH-D-15-0067.1>



*Example of surface elevation as measured from the MASS during a 2011 experiment in the Gulf of Mexico, flying above NDBC buoy #42040. (wind~12m/s, Hs = 3.1m)*

## Instrumentation

Scanning Waveform Lidar Riegl Q680i

Long-wave IR Camera FLIR SC6000 (QWIP) Ocean surface processes, wave kinematics and breaking, frontal processes

High-Resolution Video JaiPulnix AB-800CL Ocean surface processes, wave kinematics and breaking, frontal processes

Hyperspectral Camera Specim EagleAISA Ocean surface and biogeochemical processes

GPS/IMU Novatel SPAN-LN200

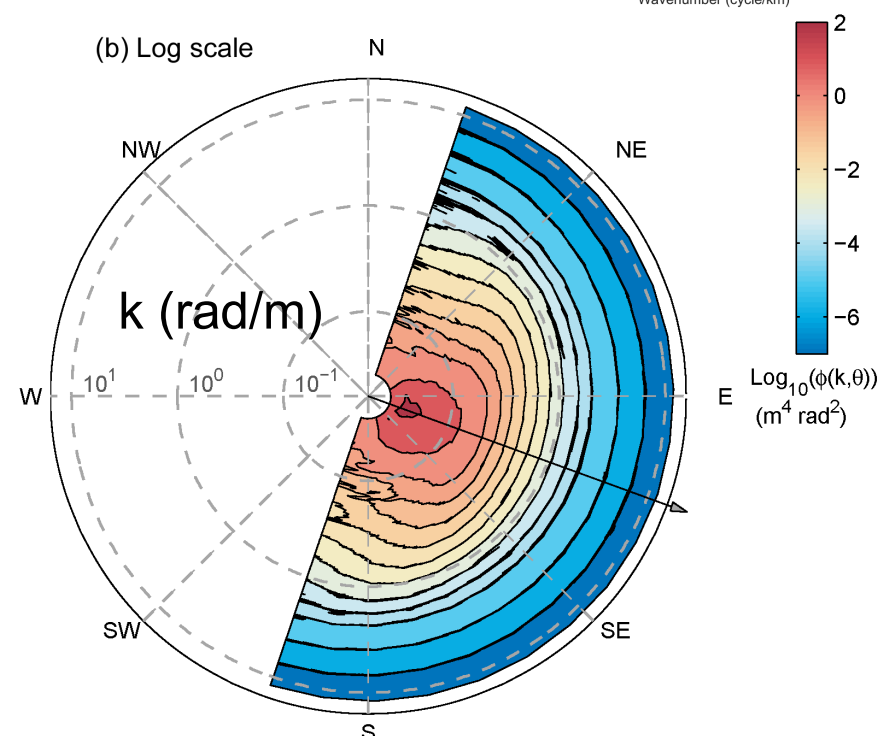
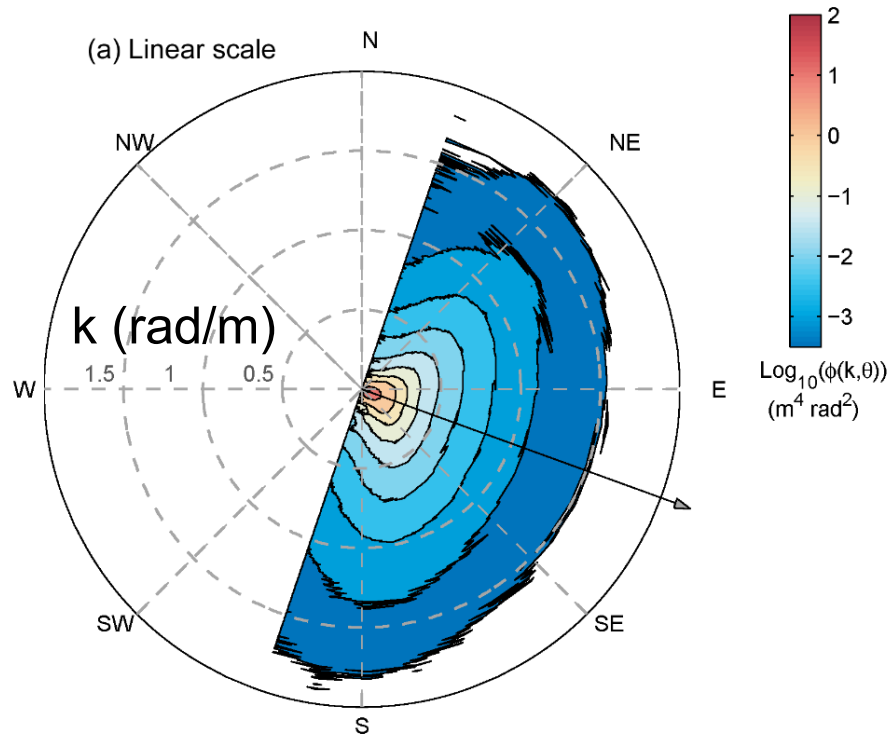
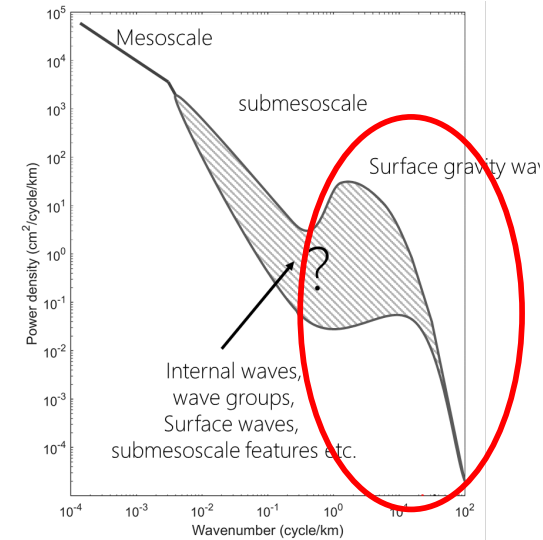
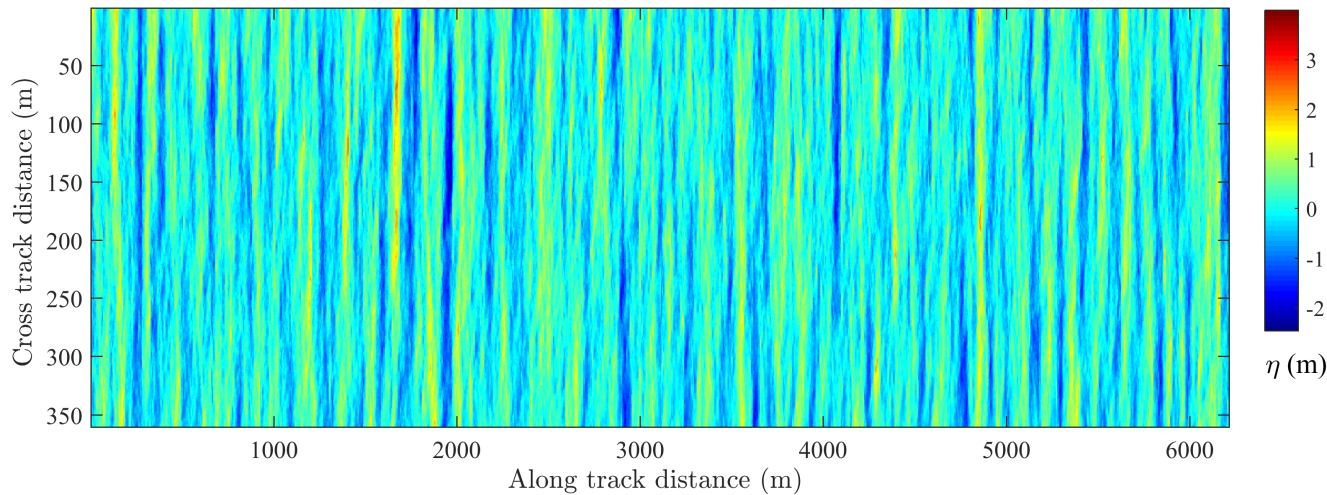
## Measurement

SSH, surface wave, surface slope, directional wave spectra (vert. accuracy ~2-3cm)

Georeferencing, trajectory

# Directional wave measurements down to sub-meter scales

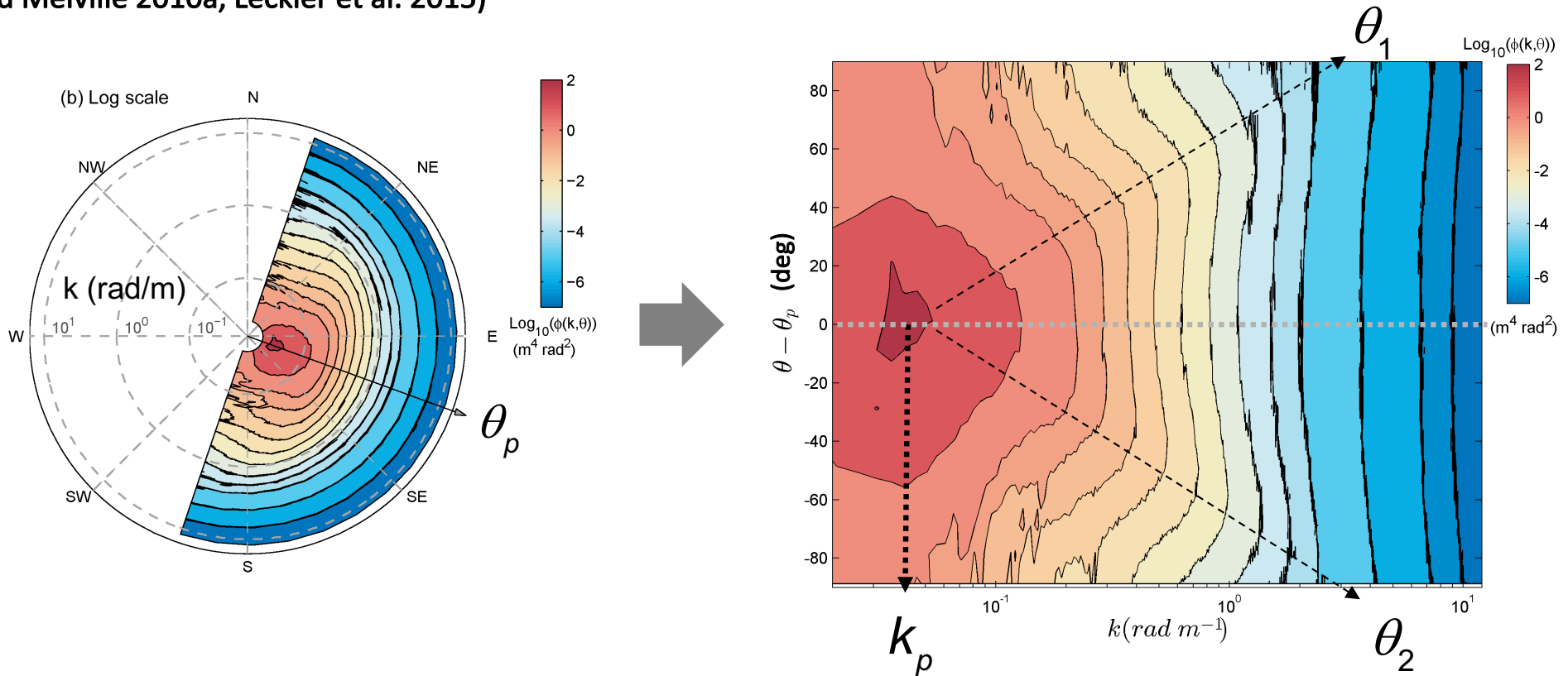
## Sea surface topography collected from MASS lidar



Lenain, L. and W.K. Melville, 2017: Measurements of the Directional Spectrum across the Equilibrium Saturation Ranges of Wind-Generated Surface Waves. *J. Phys. Oceanogr.*, 47, 2123–2138, <https://doi.org/10.1175/JPO-D-17-0017.1>

# Bimodal distribution of the directional wavenumber spectrum

Bimodality of directional wave spectrum found in earlier work for smaller wavenumbers (Hwang et al. 2000a,b; Romero and Melville 2010a, Leckler et al. 2015)



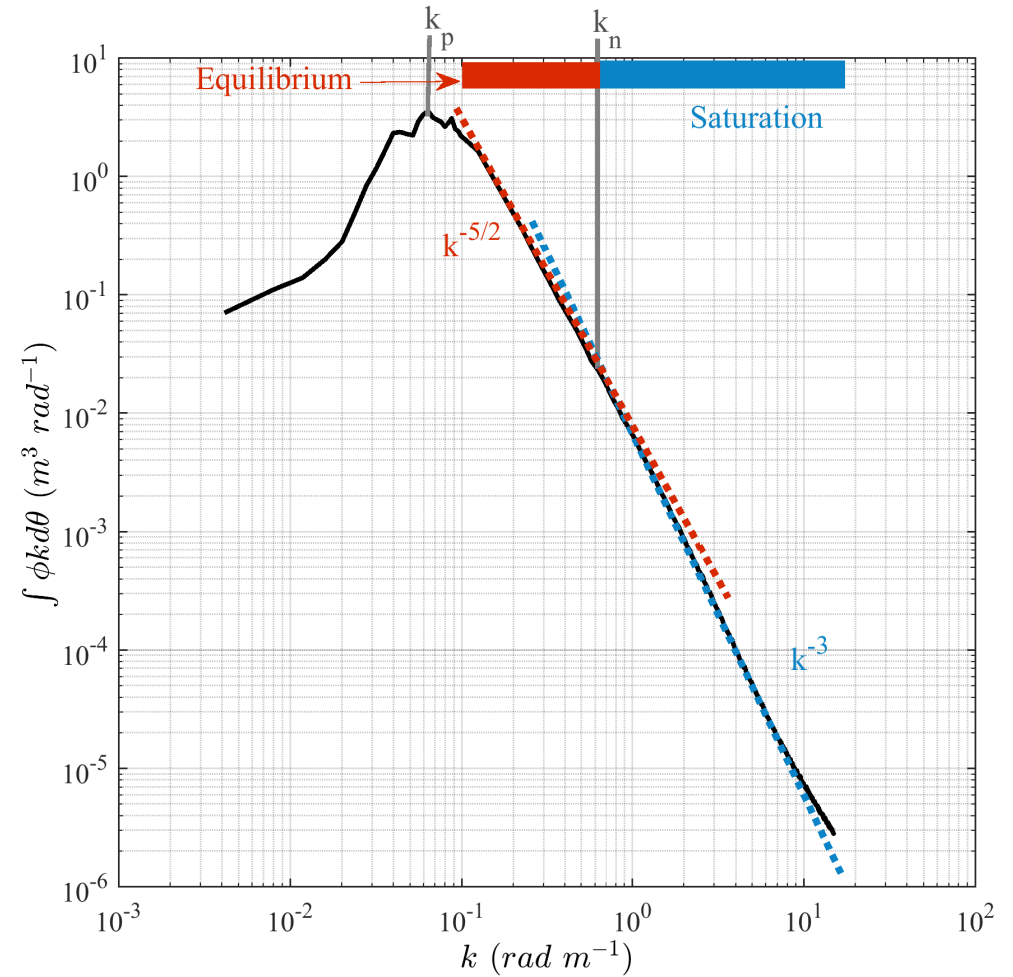
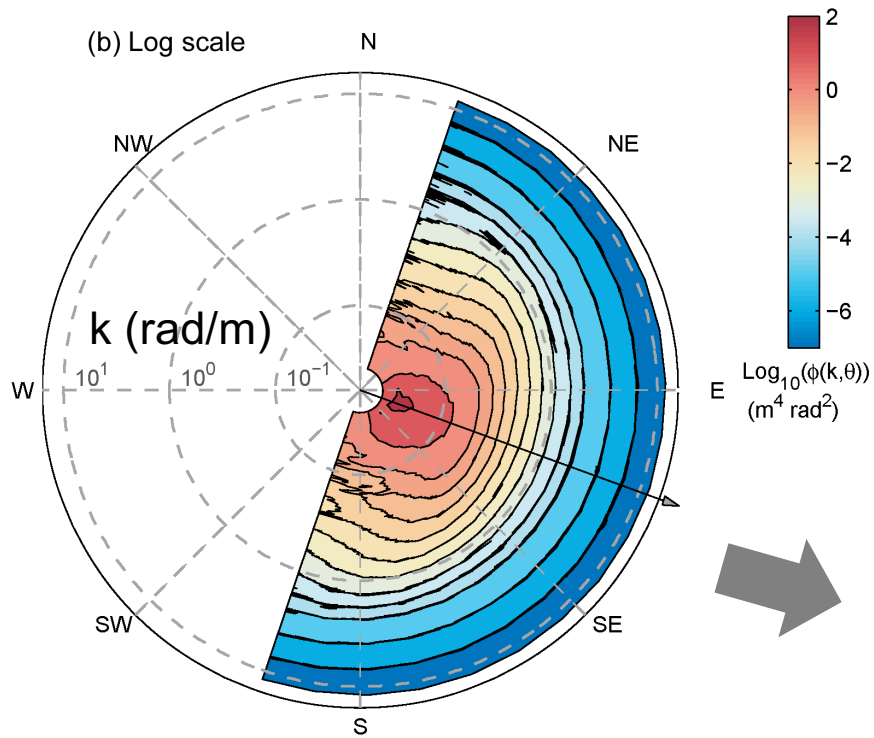
Azimuthal lobe separation

$$\theta_{lobe} = \frac{|\theta_1 - \theta_2|}{2}$$

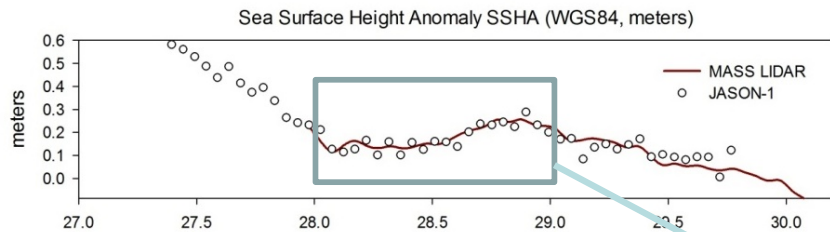
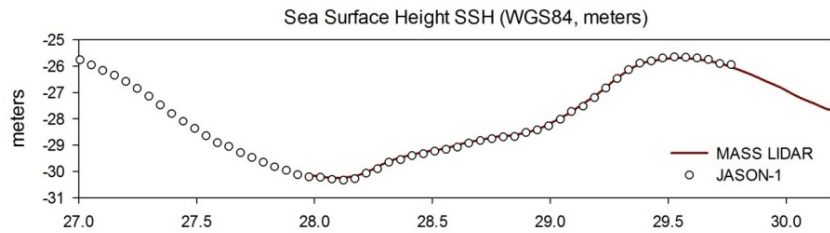
Average lobe amplitude relative to the spectral energy in the dominant wave direction

$$r_{lobe} = \frac{|\phi(k, \theta_1) + \phi(k, \theta_2)|}{2\phi(k, 0)}$$

# Example of omnidirectional wavenumber spectrum

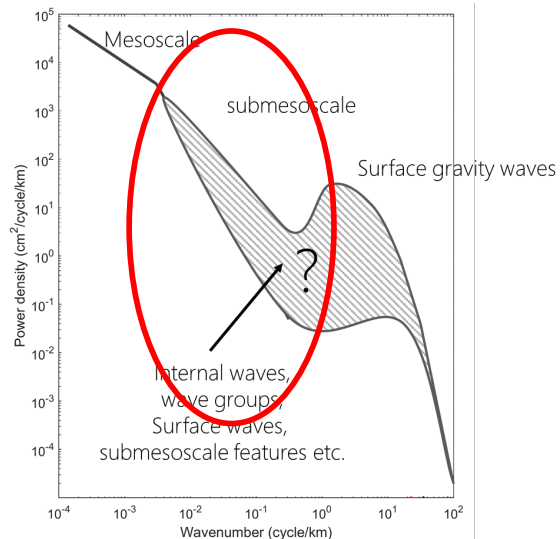
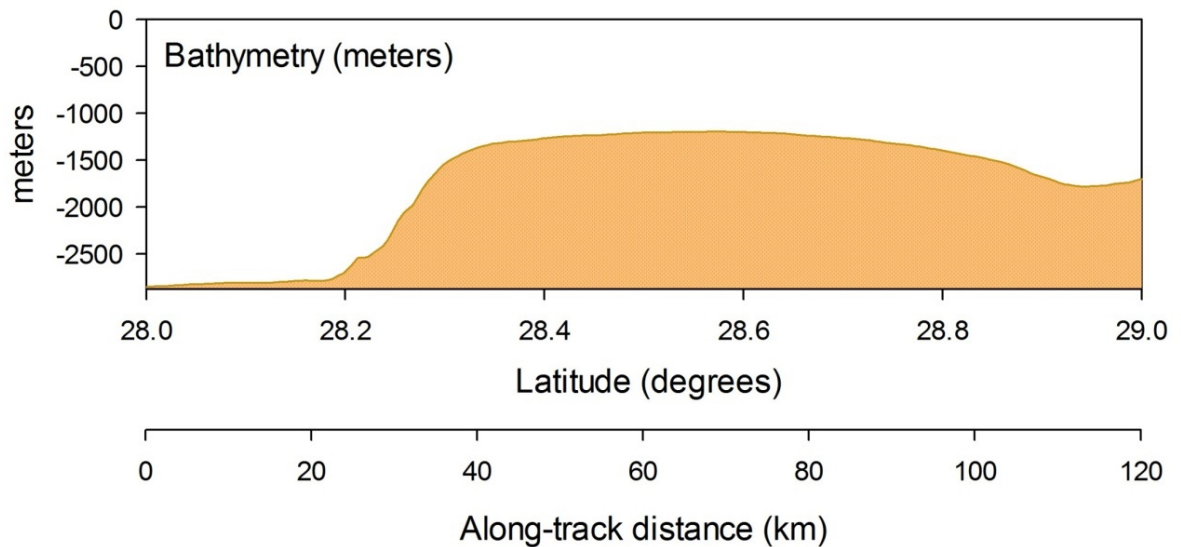
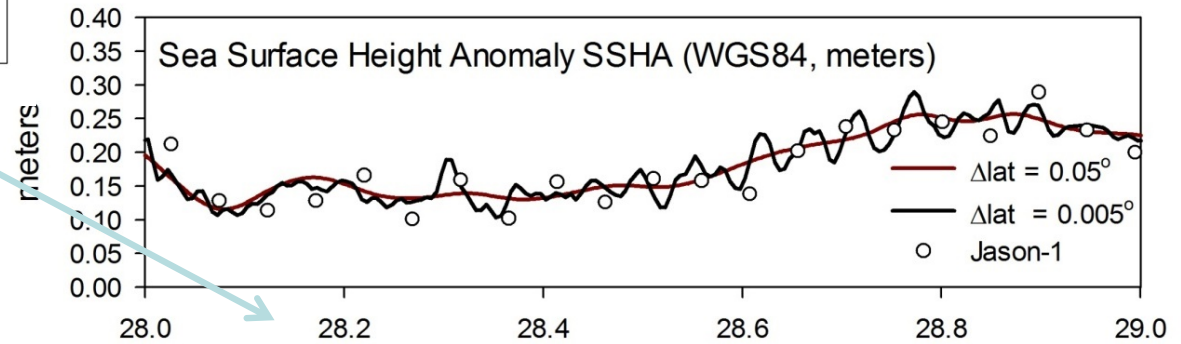


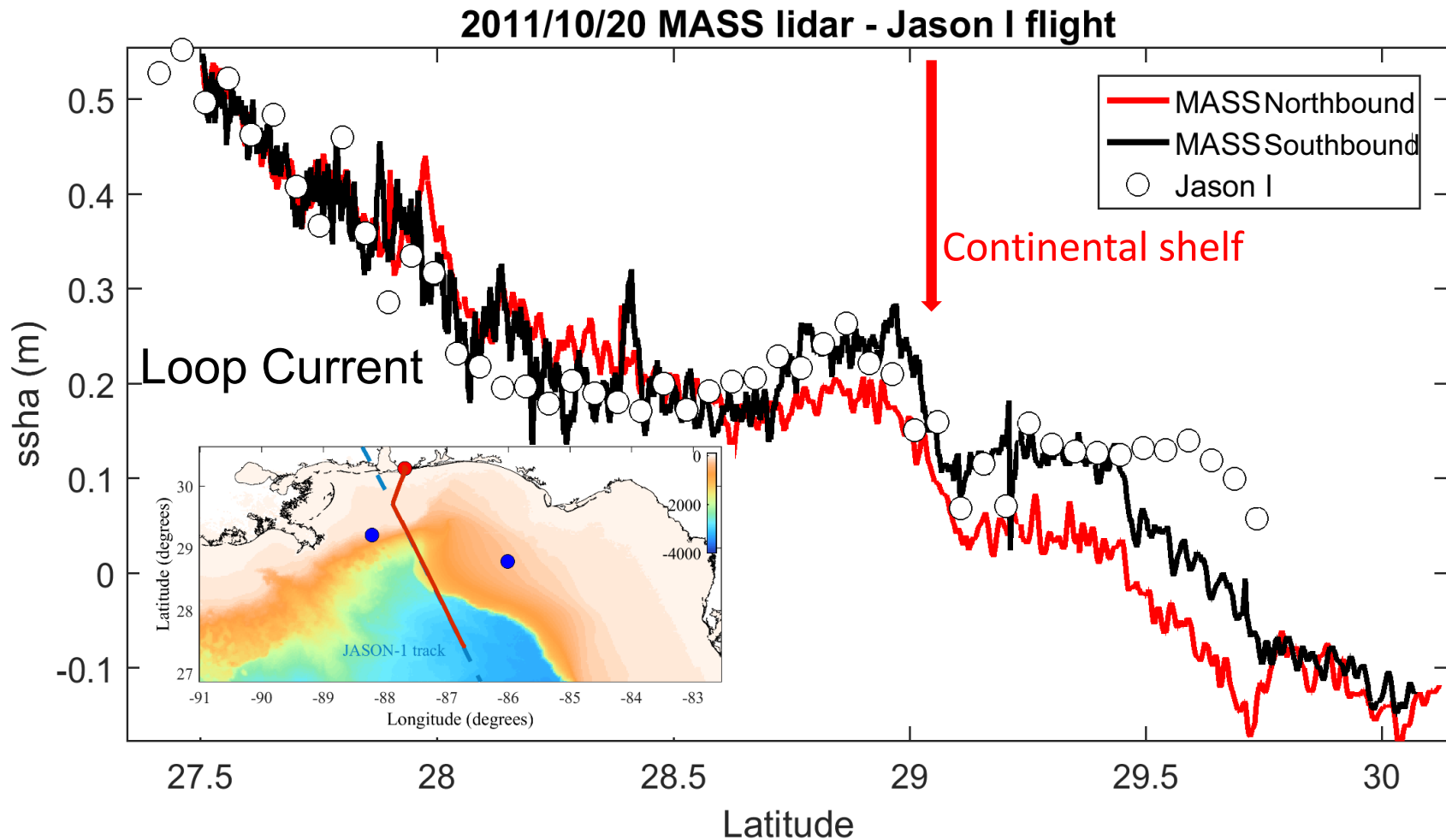
Consistent with Phillips 1985 equilibrium model and the  $k^{-3}$  saturation range



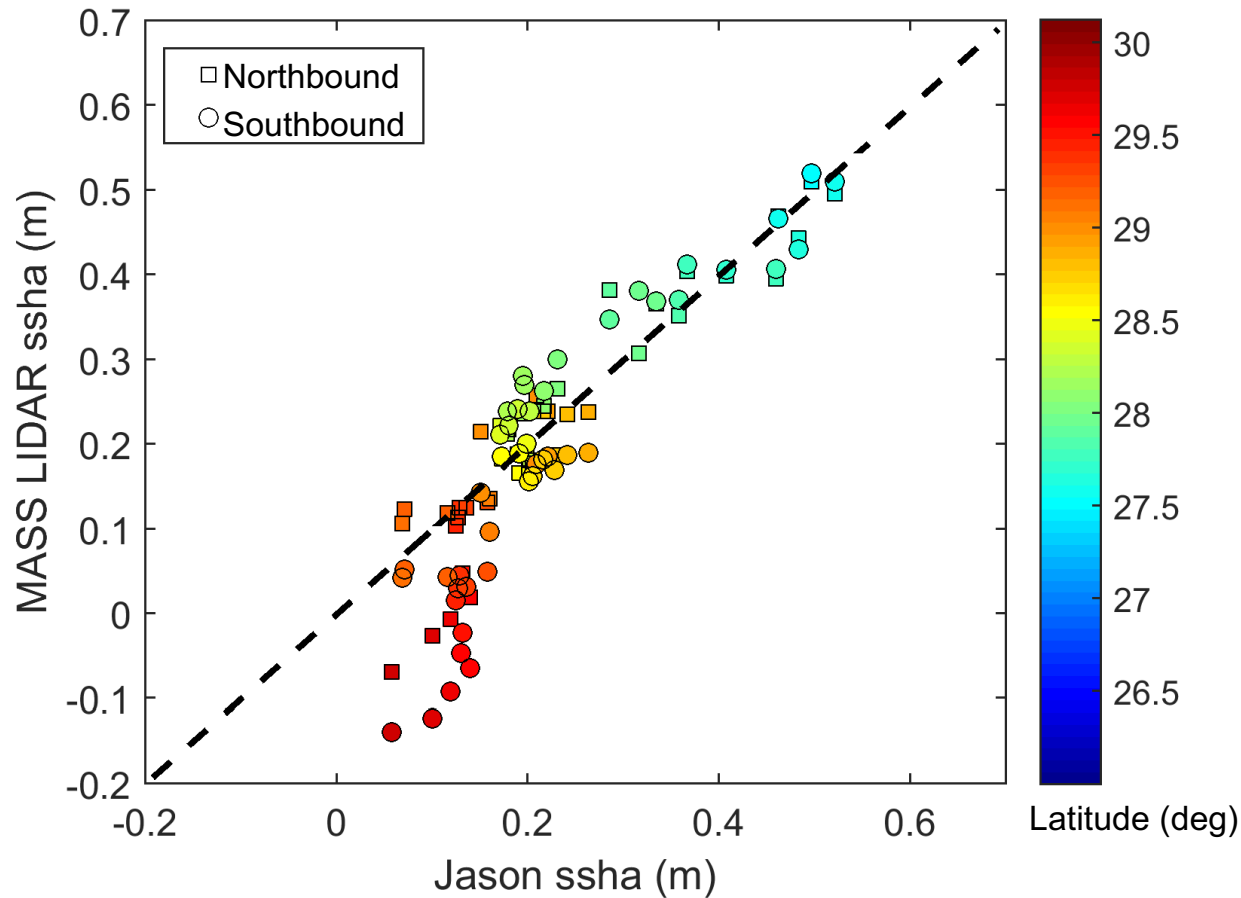
**DeSoto Canyon, Gulf Mexico 2011 Experiment**  
 (from Melville et al. 2016 JTECH publication).

**Lidar is capturing real phenomena at wavelengths shorter than observed by existing radar altimeters; SWOT will explore these effects, so Cal/Val at these scales is critical.**



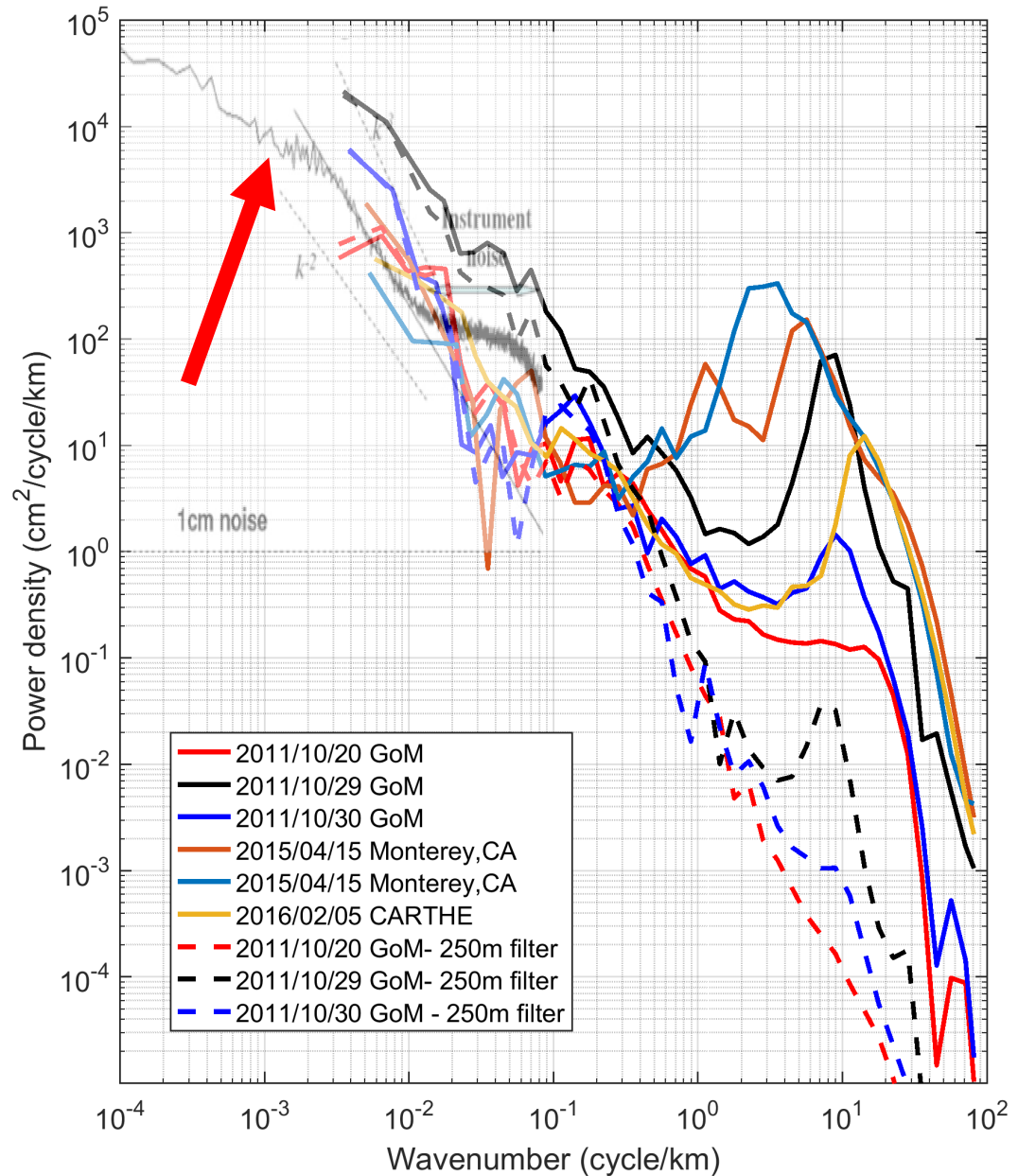


SSHA estimated from two MASS lidar passes (“northbound” and “southbound”) over the same Jason-I track (see insert). Note that the satellite pass occurred in the middle of the southbound lidar pass (black).



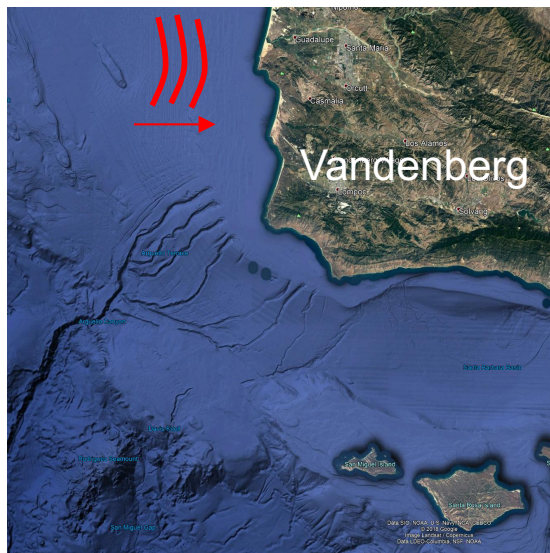
Scatterplot of the SSHA measured by Jason-I and the MASS lidar averaged over the along-track spatial resolution of the satellite for the latter. Note the divergence for the northern part of the track, as we get close to the continental shelf.

SSHA spectra measured by the MASS scanning lidar for the flights conducted during the three experiments: GoM2011, Monterey2015 and CARTHE 2016 (GoM). The data are plotted over satellite altimeter data from Figure 1 of Fu & Ferrari (2008), noting the O(100)km resolution of the traditional satellite altimeters.



# Modulation of surface gravity waves by internal waves

## ONR Innershelf DRI, September 2017



Internal wave packet propagation to the East on September 13<sup>th</sup> 2017

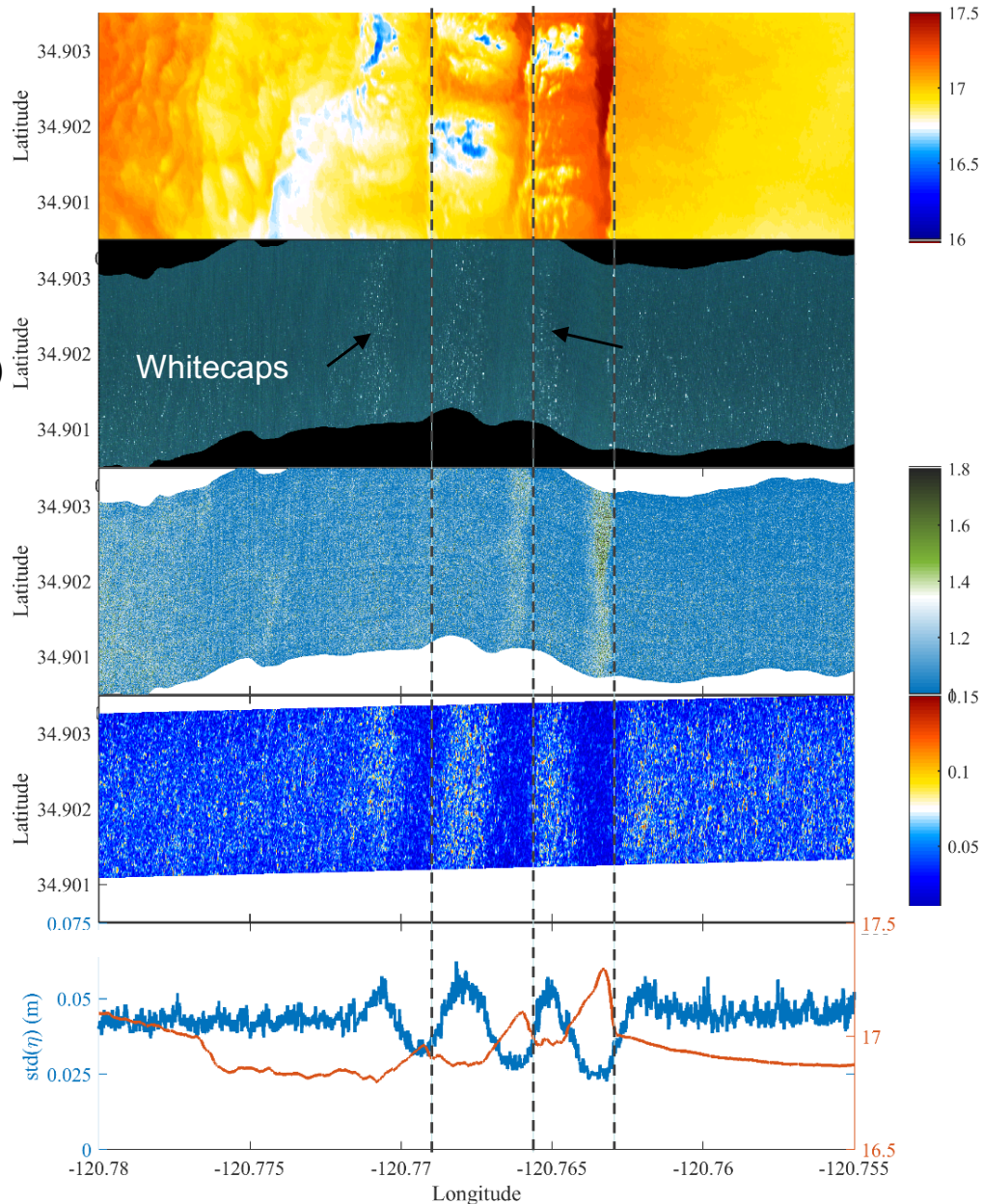
SST(°C)

Ocean Color (RGB) & Whitecaps

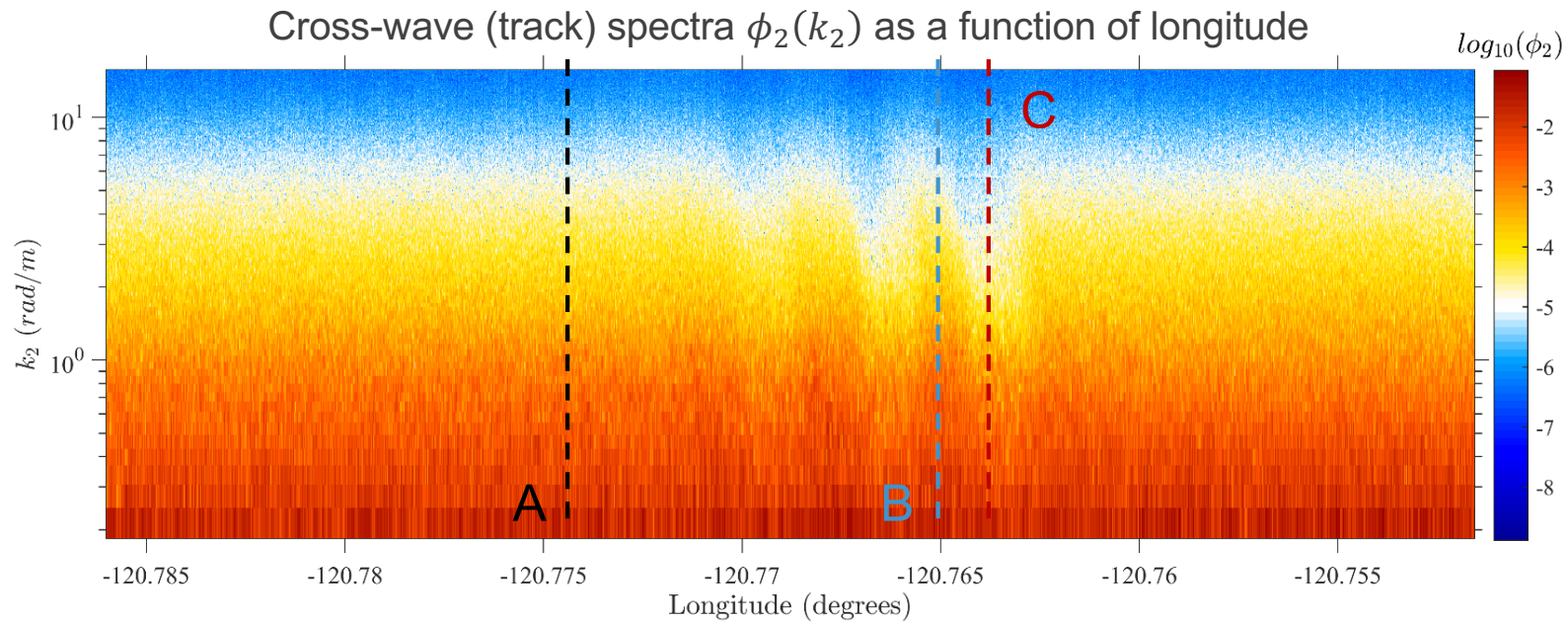
Chlorophyll-a (mg/m<sup>3</sup>)

$\text{std}(\eta)$  (m) over 2m squares (represents the very high wavenumber part of the wave spectrum)

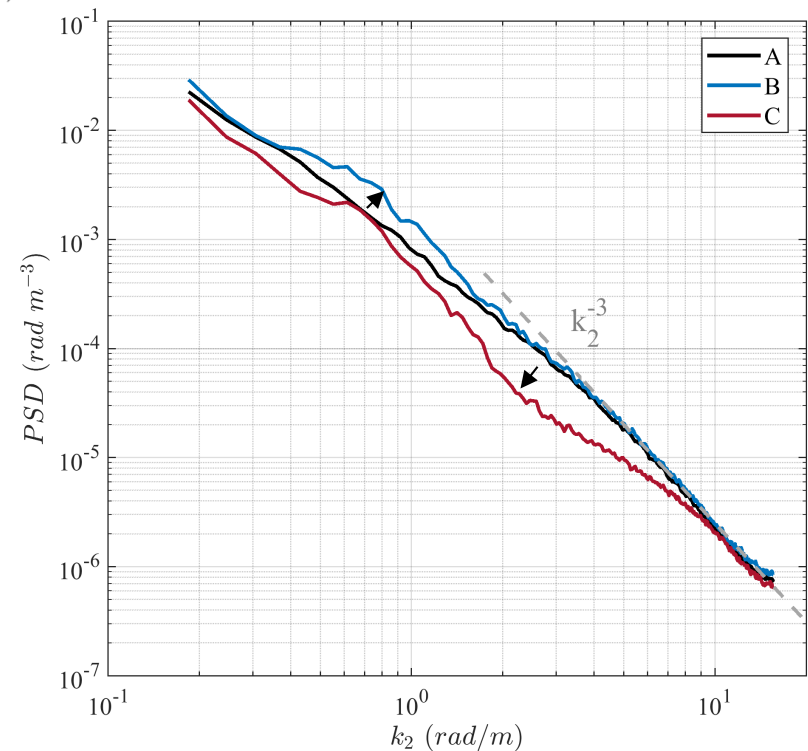
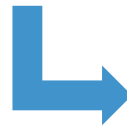
$\langle \text{std}(\eta) \rangle$  &  $\langle \text{SST} \rangle$  (cross-track averaged)



Note the modulation of the surface wave field by the IWs (smooth/rough bands sequence) and the focusing of surface chlorophyll on the forward faces of the waves.



Modulation of the surface  
wave field by the propagating  
internal waves



- We have shown that airborne lidar can measure SSH from mesoscales down to submeter scales.
- The Riegl lidar in the SIO MASS system has a swath width up to 1 km wide with a horizontal bandwidth that depends on the speed and range of the aircraft. For example, the light twin aircraft (Partenavia P68) has a cruise speed of 200 km/hr and a range of 1000 km, giving submeter resolution out to wavelengths of  $O(200)$  km. On the other hand a Gulfstream GV business jet has a cruise speed of 900 km/hr and a range of, 12,000 km, giving  $O(1)$  m resolution out to wavelengths of several thousand kilometers.
- Reciprocal flights over sand dunes (effectively stationary topography, not shown here) suggest that the largest errors, which are still within SWOT cal/val requirements, are due to GPS positioning data.
- Ocean data support the significance of surface waves, em bias and wave groups with horizontal scales out to kilometers.
- Also significant are internal waves which are shown to modulate the lidar backscatter as they do other electromagnetic scattering, including microwave and thermal infrared.

